Article

Reliable Online Internal Short Circuit Diagnosis on Lithium-Ion Battery Packs via Voltage Anomaly Detection Based on the Mean-Difference Model and the Adaptive Prediction Algorithm

Rui Cao [1], Zhengjie Zhang [1], Jiayuan Lin [1], Jiayi Lu [1], Lisheng Zhang [1], Lingyun Xiao [2], Xinhua Liu [1] and Shichun Yang [1,*]

[1] School of Transportation Science and Engineering, Beihang University, Beijing 102206, China
[2] China National Institute of Standardization, Beijing 100084, China
[*] Correspondence: yangshichun@buaa.edu.cn

Abstract: The safety issue of lithium-ion batteries is a great challenge for the applications of EVs. The internal short circuit (ISC) of lithium-ion batteries is regarded as one of the main reasons for the lithium-ion batteries failure. However, the online ISC diagnosis algorithm for real vehicle data remains highly imperfect at present. Based on the onboard data from the cloud battery management system (BMS), this work proposes an ISC diagnosis algorithm for battery packs with high accuracy and high robustness via voltage anomaly detection. The mean-difference model (MDM) is applied to characterize large battery packs. A diagram of the adaptive integrated prediction algorithm combining MDM and a bi-directional long short-term memory (Bi-LSTM) neural network is firstly proposed to approach the voltage prediction of each cell. The diagnosis of an ISC is realized based on the residual analysis between the predicted and the actual state. The experimental data in DST conditions evaluate the proposed algorithm by comparing it with the solo equivalent circuit-based prediction algorithm and the Bi-LSTM based prediction algorithm. Finally, through the practical vehicle data from the cloud BMS, the diagnosis and pre-warn ability of the proposed algorithm for an ISC and thermal runaway (TR) in batteries are verified. The ISC diagnosis algorithm that is proposed in this paper can effectively identify the gradual ISC process in advance of it.

Keywords: lithium-ion batteries; the cloud battery management system (BMS); internal short circuit (ISC); voltage prediction; thermal runaway (TR)

1. Introduction

The market sharing of electrical vehicles is rising rapidly in recent years in the worldwide automobile market due to its performance superiorities such as energy conservation and environmental friendliness [1,2]. However, the safety concerns of lithium-ion batteries still exist [3,4]. The TR risk is the main reason for lithium-ion battery safety issues [5,6]. Annually, there are several uncontrollable fire accidents in EVs that are caused by battery TR. An ISC is generally regarded as one of the main factors that trigger thermal abuse in random use conditions. It is of vital importance to realize the online monitoring of the micro internal short circuits of batteries for reducing vehicle fire accidents [7,8].

The TR process that is caused by ISCs is divided into three stages according to the changes of the macro voltage, temperature, and the corresponding protection [9]. The concepts were also reviewed in the work [10]. In actual working conditions, due to the lack of thermocouples and the hysteresis of over-heat sensing, it is difficult to realize the accurate monitoring and prewarning of thermal abuse. Many researchers confirm that the ISC occurs when it is accompanied by different abuse conditions. Maleki et al. [11] investigated the effects of an ISC based on the combination of thermal modeling and experimental methods.

The results in the work showed that the batteries with a larger capacity and a higher charge cut-off voltage and SOC have an increased risk of ISC. Gao et al. [12] proposed an ISC diagnosis method using a mean-different equivalent circuit model on a series battery pack model. Huang et al. [13] observed the in situ image of the ISC process after disassembly. The work confirms that the internal micro short circuit increased when the voltage dropped suddenly, while the ISC would aggravate the abnormal voltage dropping inversely and lead to battery self-discharge. In previous studies, the ISC diagnosis of batteries pack in real working conditions is hardly ever discussed. Due to the limitations of the online applications, the ISC diagnosis of packs needs to meet the requirements of accuracy and computational feasibility. In this work, the ISC diagnosis strategy is based on battery pack modeling, which reduces the required calculation parameters significantly, while ensuring accuracy. In addition, it is generally believed that the voltage of lithium-ion batteries has the most intuitive macro performance of the ISC in the batteries. For practical vehicle data, the voltage is the battery state with the lowest measurement cost and the highest measurement accuracy, at present [14]. In the practical detection process, the slight sudden drop and gradual drop of the voltage leading to an ISC are hard to monitor [15,16]. Therefore, it is necessary to develop an adaptive ISC diagnosis algorithm based on the battery voltage.

The ISC diagnosis and warning strategies can be broadly divided into threshold-based, model-based, and data-driven methods. The threshold-based methods realize the ISC warnings based on the comparison of the monitoring variables and the corresponding thresholds, which are the easiest to be implemented. However, it is difficult to achieve prewarning using fixed thresholds in random working conditions. To extend the number of monitoring factors, many researchers proposed entropy variables such as information entropy [17], modified sample entropy [18], and Shannon entropy [19] to attain a real-time multi-fault diagnosis. The model-based methods are more accurate in characterizing the behavior of battery packs, while in actual dynamic conditions, it is challenging to accomplish its parameter identification. Wang et al. [20] proposed a high-fidelity equivalent circuit model for an insulation fault diagnosis. Schimid et al. [21] used an equivalent circuit model for a battery pack combined with extra switches to realize the fault diagnosis and the isolation data. The data-driven methods were applied widely in the fault detection area. Trained by rich sample data, the neural network could realize complex state regressions and achieve model solving. There being a lack of sample data with definite training labels considering the nonlinear properties and the measurement noise are the limitations of the data-driven methods of ISC prewarning. Li et al. [22] proposed an ISC warning framework combing the recurrent network and the equivalent model to diagnose the abnormal voltage. Zhao et al. [23] combined the BP network with big data statistical regulation to construct a fault detection model for the battery system. However, most of the model-based methods were calibrated by experimental data. So, the feasibility of these methods in real working conditions needs to be further improved. An online ISC diagnosis and prewarning algorithm enabling its implementation on the cloud BMS is of significance [24,25].

This work innovatively proposes an online pack ISC diagnosis method based on an adaptive integrated prediction algorithm in the application scenario of random working conditions. The core logic of ISC diagnosis in this work is evaluated by the residual analysis between the predicted state and the real state of the packs. To achieve a high-precision state prediction, a diagram of an adaptive integrated prediction algorithm combining equivalent circuits and neural networks is, firstly, proposed. The ISC diagnosis operates online on the battery cloud platform and the input and output are connected to the database and visualized platform. The online data are from passenger cars using NMC batteries in 2021. Considering the feasibility of online monitoring and the effectiveness of the macro variables, the voltage of the battery packs is chosen as the main analysis object to monitor the abnormal self-discharge.

In this paper, the proposed algorithm firstly realizes the ISC detection of large battery packs in real vehicles and is verified by the online cloud-side data. The determination of the algorithm discriminant factors combines the equivalent circuit model of the battery

pack, the cyclic neural network, and integrated learning. The concerns of the overfitting and there being a low accuracy for the algorithm are resolved. The model of this method is trained by a large volume of online data in real working conditions. The computational logic of the state of cells in the battery packs is based on the MDM. The computing resource requirement of this method is reduced greatly. The hard-to-detect slight drops and gradual drops, leading to ISCs, are detected in the validation process, which proves the competent performance of the proposed method in practical applications.

The rest of the paper is organized as follows. The model of the battery pack and identification process are discussed in Section 2. The pack voltage prediction algorithm and corresponding test are introduced in Section 3. Based on actual vehicle data from the cloud platform, the proposed prediction framework is presented and validated in Section 4. The conclusions and perspectives of this work are discussed in Section 5.

2. Battery Pack Modeling Based on the MDM

The modeling of battery packs plays an important role for the cell state estimation and prediction. The MDM of battery packs was proposed in previous work [26]. The superiority of the MDM is that it has a high accuracy with low requirements for computing resources. The MDM can not only describe the mean state of the battery pack, but also focus on the inconsistency of each cell, which makes it advantageous to be applied to the analysis of a large battery pack. Gao et al. [27] evaluated four types of battery pack models. In the work, the practicability of the MDM was proved, and MDM#2 was applied in the battery fault identification test. In the MDMs, the battery pack is seen as an assembly of one CMM (cell mean model) and several CDMs (cell different models). The physical meaning of the CMM is the approximate average state of the whole pack, while the CDMs represent the corresponding difference between the single cell state and the cells' mean state. The first-order Thevenin model is usually selected as the cell mean model. The CDMs are mainly divided into four categories according to the difference in their consider deviation quantities. The number of the considered deviation variables determines the accuracy, robustness, and computational complexity of the MDMs.

Figure 1 shows the four categories of MDMs according to the number of unknown variables. Among the four kinds of CDMs, CDM#4 is considered to be the most accurate model due to it having the largest number of considering variables, but the computational complexity of the model has exceeded that of the first-order Thevenin model. Considering the difference in cell capacity, the identification of the CDM #3 model often depends on an accurate SOC-OCV relationship calibration and SOC estimation, which makes it difficult to be applied in the actual working conditions of large battery packs. CDM#1 and CDM#2 are most widely used ones at present. Compared with CDM#1, CDM#2 has more application significance for cell ISC detection considering the difference in the ohmic internal resistance of the battery's aging.

In this work, CDM#2 is chosen as the model of the cell difference due to it having a high accuracy and low requirement in terms of the computational effort. The polarization parameters R_p and C_p are simplified in MDM#2, which improves the robustness of the model in real working conditions. Modeled by MDM#2, the unknown parameters in the battery pack were reduced by almost 2/3, especially in the battery pack with more than 100 cells. The state functions of MDM#2 are shown in Table 1. In the process of model identification, the relationships between the SOC, OCV, and the temperature, and the SOC_{mean}, ΔSOC, and ΔOCV are the main part of the model observation equation. Figures 2 and 3 show the SOC–Temperature–OCV three-dimensional schematic of the NMC batteries and SOC_{mean}–ΔSOC–ΔOCV three-dimensional schematic of the CDM#2, respectively.
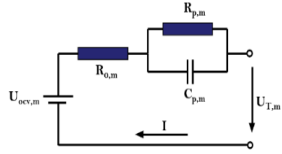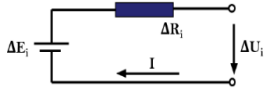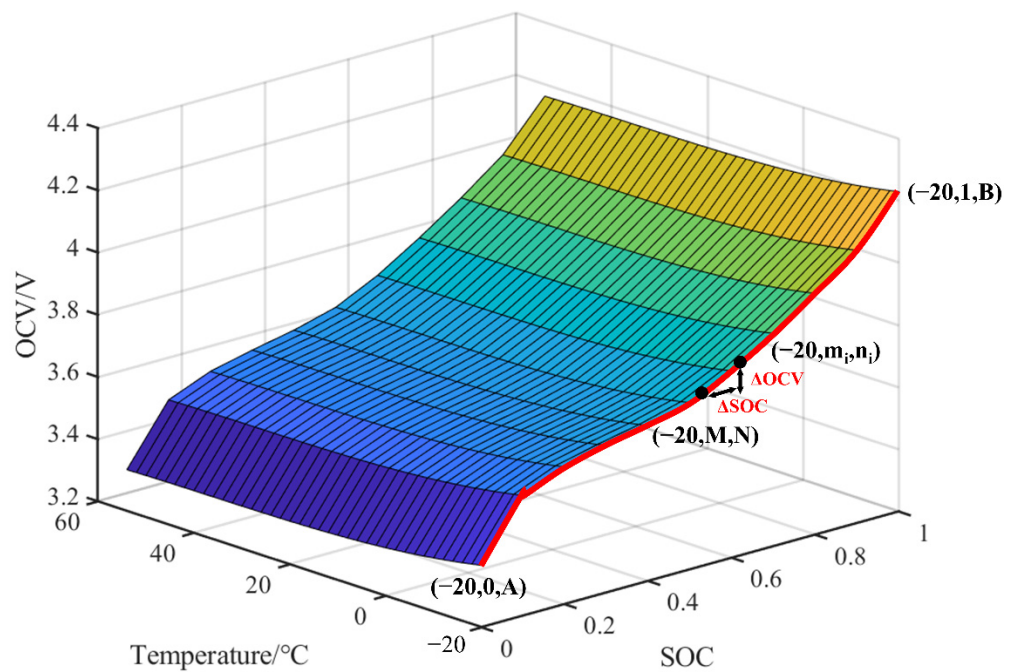
Figure 1. MDMs with different CDMs.

Figure 2. SOC–Temperature–OCV three-dimensional schematic of the NMC batteries.

Table 1. State equations of MDM#2 model [12].

|	**State Equations**
	$\dot{U}_{P,m} = -\frac{1}{R_{P,m}C_{P,m}}U_{P,m} + \frac{1}{C_{P,m}}I$ $U_{T,m} = U_{OCV,m} - U_{P,m} - R_{O,m}I$ where $U_{T,m}$ represents the mean terminal voltage of the battery pack, $R_{P,m}$ and $C_{P,m}$ are the polarization internal resistance and polarization capacitance, respectively, $U_{P,m}$ is the polarization voltage, $R_{0,m}$ represents the ohm internal resistance, and I is the instantaneous current. $U_{OCV,m}$ represents the OCV. $\Delta U_{T,i} = \Delta U_{OCV,i}(\Delta SOC_i) - \Delta R_{0,i}I$ where $\Delta U_{T,i}$, $\Delta U_{OCV,i}$, ΔSOC_i, and $\Delta R_{0,i}$ represent difference of corresponding parameters between the cell i and mean battery model and I is the instantaneous current.
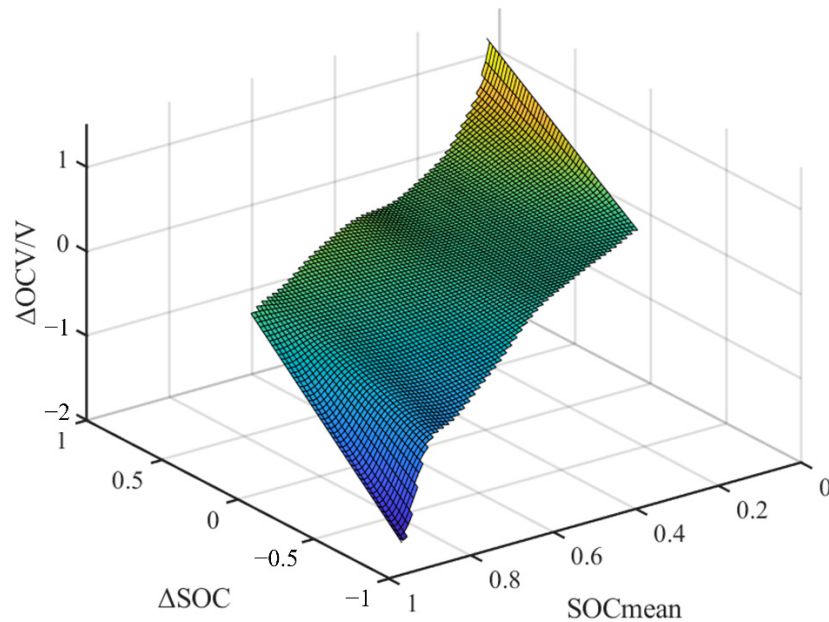
Figure 3. SOCmean–ΔSOC–ΔOCV three-dimensional schematic of the CDM#2.

In Figure 2, OCV is set as a function of SOC and the temperature, where SOC and temperature are two independent variables. Considering the influence of SOC and the temperature on OCV, they will improve the accuracy of the model to a certain extent. Compared with the single OCV–SOC curve, the accuracy of the model is improved due to the additional consideration of the temperature variables. Mapping the relationship between Figures 2 and 3 can be discussed as follows. In Figure 2, the red line is the OCV–SOC curve when the temperature is $-20\,^{\circ}$C. According to the relative position of the two points $(-20, M, N)$ and $(-20, m_i, n_i)$ in Figure 3, we can obtain that $m_i - M = \Delta SOC$ and $n_i - N = \Delta OCV$. Considering the actual physical meaning of SOC, we can obtain that the known constraints are $\Delta SOC + M \leq 1$ and $\Delta SOC + M \geq 0$, and the corresponding domain of function is $[0, B - A]$. In the application scenario, for the battery packs with good consistency, the ΔSOC value tends to be close to 0, and the $\Delta OCV/\Delta SOC$ is approximate to the derivative of OCV to SOC. Since the temperature is relatively independent of SOC, the influence of the temperature can be ignored.

3. Voltage Prediction Framework

In this work, a large battery pack with the configuration of 86S4P is modeled based on the MDM model. In the process of voltage prediction, in order to enhance the accuracy and

robustness of the prediction, the whole algorithm structure is based on the MDM equivalent circuit model to predict the mean and deviation state and modify the CMM prediction results by combining the vehicle state data. The input of the adaptive prediction algorithm is the vehicle state data including the speed, temperature, and mileage; the battery state data include the voltage, temperature, and current. A neural network model on voltage prediction is designed based on the onboard data. Via the AdaBoost algorithm, the ECM–RLS prediction results were fused with the results of the neural network to improve the robustness and accuracy of the overall estimation. The schematic diagram of the adaptive integrated prediction algorithm is shown in Figure 4.
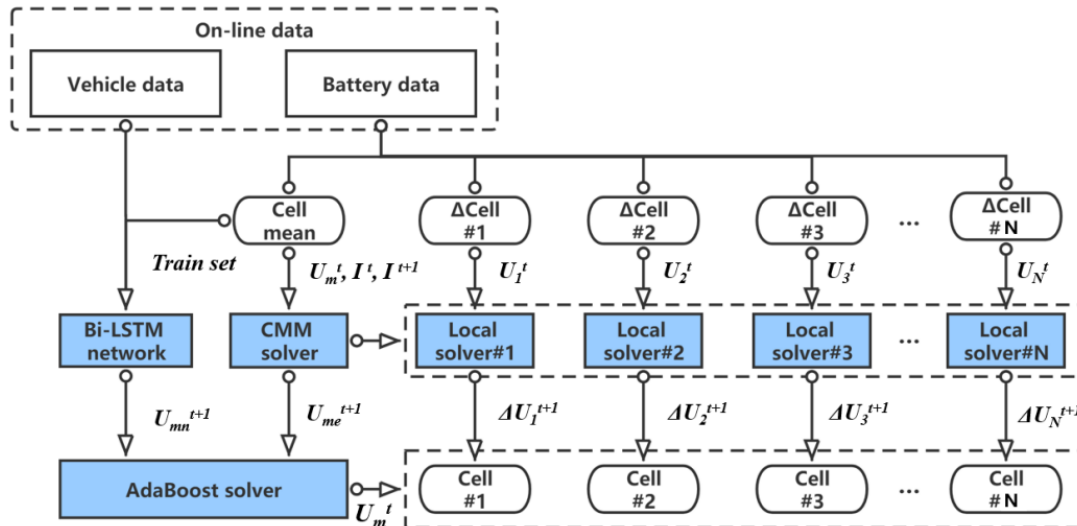

Figure 4. Schematic diagram of the adaptive prediction algorithm.

3.1. Voltage Prediction via Bi-LSTM on CMM

The mean prediction for the CMM model using the Bi-LSTM network is proposed in this work. The input of the network is made up of the vehicle and battery data, and the predicted voltages form the output. The structure and the dataset of the proposed BI-LSTM network are discussed as follows.

3.1.1. Schematic of BI-LSTM

Functionally, the memory cell of the BI-LSTM network can not only achieve long-term memory, but also avoid the gradient disappearance and explosion problem. The input information of every memory cell is comprised of the current moment input x_t, the cell state, and the hidden state h_{t-1} in $t-1$ moment, and the current moment cell state h_t and hidden state h_t form the output. The timely prediction of the LSTM is deduced by the coupling of the forget gate, input gate, and output gate in every memory cell [28]. The main computing process is shown as follows, where the weight matrix is $W = [W_f \quad W_t \quad W_o]^T$, the bias matrix is $b = [b_f \quad b_t \quad b_o]^T$. σ represents the sigmoid activation function and x_t represents the timely input [29].

$$\text{Forget gate layer}: \ f_t = \sigma(W_f \cdot [h_{t-1}, x_t] + b_f) \tag{1}$$

$$\text{Input gate layer}: \ i_t = \sigma(W_i \cdot [h_{t-1}, x_t] + b_i) \tag{2}$$

$$\widetilde{C}_t = \tanh(W_C \cdot [h_{t-1}, x_t] + b_C) \tag{3}$$

$$\text{Output gate layer}: \ o_t = \sigma(W_O \cdot [h_{t-1}, x_t] + b_o) \tag{4}$$

$$h_t = o_t \cdot \tanh(C_t) \tag{5}$$

Based on the above equations, the input and the hidden signal are corrected to produce the coupling output, which leads to high relativity between the output and the time memory. The parameters of the battery pack changed gradually as the capacity and performance decreased, which made the current status of the batteries available to be predicted by the online data with either a forward or backward time series [30]. In this section, the Bi-LSTM was chosen as the core of the constructed neural network, and an additional regression network was added to ensure its robustness. Compared with the traditional LSTM, Bi-LSTM can achieve more timely learning efficiency rates based on the bidirectional network training via the even numbers of the LSTM layers. The odd and even layers implement the forward and reversed training and coding, respectively. The deducing process is shown as follows.

Forward deducing process:

$$
\begin{cases}
\vec{i_t} = \sigma_g\left(\vec{W_i}x_t + \vec{R_i}\vec{h_{t-1}} + \vec{b_i}\right) \\
\vec{f_t} = \sigma_g\left(\vec{W_f}x_t + \vec{R_f}\vec{h_{t-1}} + \vec{b_f}\right) \\
\vec{o_t} = \sigma_g\left(\vec{W_o}x_t + \vec{R_o}\vec{h_{t-1}} + \vec{b_o}\right) \\
\vec{c_t} = \vec{f_t} \odot \vec{c_{t-1}} + \vec{i_t} \odot \tanh\left(\vec{W_e}x_t + \vec{R_e}\vec{h_{t-1}} + \vec{b_e}\right) \\
\vec{h_t} = \vec{o_t} \odot \tanh\left(\vec{c_t}\right)
\end{cases} \tag{6}
$$

Backward deducing process:

$$
\begin{cases}
\overleftarrow{i_t} = \sigma_g\left(\overleftarrow{W_i}x_t + \overleftarrow{R_i}\overleftarrow{h_{t-1}} + \overleftarrow{b_i}\right) \\
\overleftarrow{f}_t = \sigma_g\left(\overleftarrow{W_f}x_t + \overleftarrow{R_f}\overleftarrow{h_{t-1}} + \overleftarrow{b_f}\right) \\
\overleftarrow{o_t} = \sigma_g\left(\overleftarrow{W_o}x_t + \overleftarrow{R_o}\overleftarrow{h_{t-1}} + \overleftarrow{b_o}\right) \\
\overleftarrow{c_t} = \overleftarrow{f}_t \odot \overleftarrow{c_{t-1}} + \overleftarrow{i_t} \odot \tanh\left(\overleftarrow{W_e}x_t + \overleftarrow{R_e}\overleftarrow{h_{t-1}} + \overleftarrow{b_e}\right) \\
\overleftarrow{h_t} = \overleftarrow{o_t} \odot \tanh\left(\overleftarrow{c_t}\right)
\end{cases} \tag{7}
$$

The output of the network can be deduced as $y_t^* = W_r(\vec{h_t} \odot \overleftarrow{h_t}) + b_r$. The schematic diagram of the network is shown in Figure 5. The loss function of the whole network including the Bi-LSTM and regression network is the optimization of the mean squared error, which can be shown as follows.

$$
loss = 0.5\sum_{i=1}^{t}\left(y_i^* - x_i\right)^2 \tag{8}
$$

where y_i^* represents the predicted signal and x_i means the input signals [31].
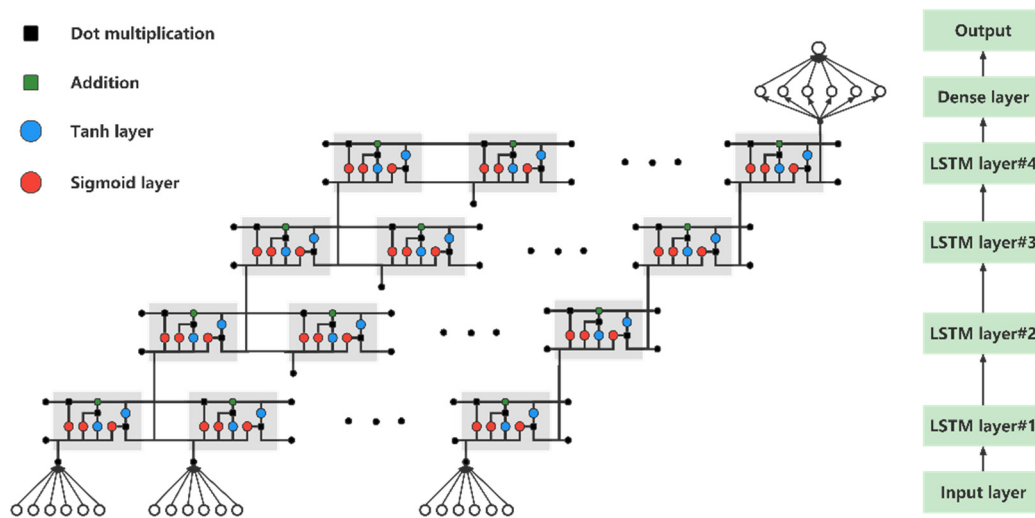
Figure 5. Schematic diagram of BI-LSTM in this work.

3.1.2. Discussion on Input Dataset for Neutral Network

Due to the fact that the macro performance of the lithium-ion batteries could be concerned with the multi-field coupling reactions, it should be considered that the inputs of the predicting model need to contain both the batteries attenuation data over time and the time-series data of the batteries and vehicles [32]. In this work, the data sources that contain the battery data and vehicle data could be obtained from the online cloud platform for the EVs. Specifically, the data for the batteries contains the pack voltage, pack current, pack SOC, isolation impedance value, pack temperature, cell voltage, and battery charge status. The vehicle data includes the mileage, speed, the status of gear, acceleration pedal, etc. The inputs of the network contain the mean temperature value, vehicle velocity, mileage, total voltage value, current value, CMM voltage value, and value of pack SOC. The training data are intercepted from the history data of normal, used vehicles. Moreover, the sampling interval of the chosen data is 30 s, which could sufficiently prove the robustness and feasibility of the proposed algorithm.

3.2. Cell Voltage Prediction Based on the MDM

Compared with the data-driven algorithm, the superiority of the equivalent circuit model for prediction could limit the sudden change of the predicting results, and the predicted results are more explicable. The unknown parameters R_0, R_P, C_P, and ΔR_0 in MDM#2 need to be identified using the real-time voltage and current. The modeling process includes the identification and parameter updating of CMM and CDM#2, in turn. Before the parameter identification of the algorithm can take place, it is necessary to discretize the MDM#2 model and deduce the model into the form of $y_i = \Phi_i \theta_i$. The main derivation process of CMM could be calculated as follows:

$$\begin{cases} \beta_1 = exp(-\Delta t/\tau) \\ \beta_2 = -R_0 \\ \beta_3 = exp(-\Delta t/\tau)R_0 - (1 - exp(-\Delta t/\tau))R_{P,m} \end{cases} \tag{9}$$

$$\begin{cases} R_{0,m} = -\beta_2 \\ R_{P,m} = (\beta_1\beta_2 + \beta_3)/(\beta_1 - 1) \\ C_{P,m} = (1 - \beta_1)\Delta t/((\beta_1\beta_2 + \beta_3)\ln(\beta_1)) \end{cases} \tag{10}$$

$$\begin{cases} y_i = E_{T,i} \\ \phi_i = [E_{T,i}\ I_i\ I_{i-1}] \\ \theta_i = [\beta_1\ \beta_2\ \beta_3]^T \end{cases} \tag{11}$$

where Δt represents the sampling interval, $\tau = R_P C_P$, and $E_T = U_T - U_{OCV}$. The derivation process of the CDM#2 model is similar, and the derivation result could be described as follows:

$$\begin{cases} y_i = E_{T,i} \\ \phi_i = [E_{T,i}\ I_i\ I_{i-1}] \\ \theta_i = [\beta_1\ \beta_2\ \beta_3]^T \end{cases} \tag{12}$$

In this section, RLS with a forgetting factor is used as the identification algorithm. RLS shows high robustness and stability for online parameter identification. The RLS algorithm with a forgetting factor is used to enhance the tracking ability of the latest state [27]. The MDM status prediction via RLS is based on the posterior estimation of every step and the correction of it by the timely current input. Table 2 shows the process of the parameter identification covering the algorithm initialization and the iteration process of the proposed model. Additionally, accurate measurements of the voltage, current, and temperature are significantly important for the parameter identification of the model. Online data cleaning is an essential procedure to ensure the convergence of the identification results. In our work, the raw data are cleaned by threshold filtering and Gaussian filtering on both the cloud platform and the local server.

Table 2. MDM Model parameter identification and prediction.

---

(1)   Identification process of CMM:

(i)   Initialization: $\phi_m, \theta_m, K_m, P_m, \lambda, \Delta\phi_k, \Delta\theta_k, \Delta K_k, \Delta P_k$ for $i = 1, 2, 3 \cdots$

(ii)   Calculate and measure the mean voltage: $U_{T,m,i} = \sum\limits_{k=1}^{n} U_{T,k,i}/n$

(iii)   Calculate the mean cell gain matrix: $K_{m,i} = \left(P_{m,i-1}\phi_{m,i}^T\right) / \left(\lambda + \phi_{m,i}^T P_{i-1}\phi_{m,i}\right)$

(iv)   Calculate the mean cell error covariance matrix: $P_{m,i} = \left(P_{m,i-1} - K_{m,i}\phi_{m,i}^T P_{m,i-1}\right)/\lambda$

(v)   Update mean cell parameter matrix: $\theta_{m,i} = \theta_{m,i-1} + K_{m,i}\left(E_{T,m,i} - \phi_{m,i-1}^T\theta_{m,i-1}\right)$

(vi)   Update estimated voltage: $y_{m,i} = \phi_{m,i}\theta_{m,i}$

(vii)   Update estimated voltage: $y_{m,i} = \phi_{m,i+1}\theta_{m,i}$

(2)   Identification process of CDM#2:

(i)   Voltage update: $U_{T,k,i} = U_{T,k,i-1}$

(ii)   Calculate gain matrix: $\Delta K_{k,i} = \left(\Delta P_{k,i-1}\Delta\phi_{k,i}^T\right) / \left(\lambda + \Delta\phi_{k,i}^T\Delta P_{k,i-1}\Delta\phi_{k,i}\right)$

(iii)   Calculate error covariance matrix: $\Delta P_{k,i} = \left(\Delta P_{k,i-1} - \Delta K_{k,i}\Delta\phi_{k,i}^T\Delta P_{k,i-1}\right)/\lambda$

(iv)   Update parameter matrix: $\Delta\theta_{k,i} = \Delta\theta_{k,i-1} + \Delta K_{k,i}\left(\Delta E_{T,k,i} - \Delta\phi_{k,i-1}^T\Delta\theta_{k,i-1}\right)$

(v)   Update estimated voltage: $\Delta y_{k,i} = \Delta\phi_{k,i+1}\Delta\theta_{k,i}$

(vi)   Update estimated voltage: $\Delta y_{k,i+1}^{pre} = \Delta\phi_{k,i+1}\Delta\theta_{k,i}$

3.3. Cell Voltage Prediction Correction Via Adaboost Solver

The Adaboost regression method is a kind of algorithm that can achieve information integration through data training and weight optimization [33]. The inputs of the Adaboost solver are the CMM predicted status by Bi-LSTM and the MDM predicted status by RLS. The calculating process of the Adaboost algorithm is shown as follows. In the iteration process of the algorithm training, the maximum error of classifiers of the training data can be deduced as $E_t = \max|y_i - h_t(x_i)|, i = 1, 2, \ldots, m$, where the $h_t(x_i)$ represents the predicted result of the sample x_i, and y_i is the target value of x_i. The square error is chosen as the relative error of $h_t(x_i)$ in (12), and the error ratio of the classifiers can be calculated in (13).

$$e_{ti} = \frac{(y_i - h_t(x_i))^2}{E_t^2}, i = 1, 2, \ldots, m \tag{13}$$

$$e_t = \sum_{i=1}^{m} Dist_t(x_i)e_{ti} \tag{14}$$

The weight of classifiers and the data samples are updated by (15) and (16), respectively.

$$Z_t = \sum_{i=1}^{m} Dist_t(x_i)w_t^{1-e_{ti}} \tag{15}$$

$$w_t = \frac{e_t}{1-e_t} \tag{16}$$

$$Dist_{t+1}(x_i) = \frac{Dist_t(x_i)}{Z_t}w_t^{1-e_{ti}} \tag{17}$$

The strong regressor of this algorithm in every step is updated by (17).

$$H(x) = \sum_{i=1}^{m} \ln\left(\frac{1}{w_t}\right)f(x) \tag{18}$$

3.4. Prediction Results Based on DST Conditions

The conventional prediction methods for the battery's state prediction are the model-based prediction methods and the data-driven prediction methods. In this subsection, the proposed algorithm is compared with the solo equivalent circuit model (ECM) based a prediction algorithm and the Bi-LSTM based prediction algorithm. In order to prove the accuracy optimization, we chose a series battery pack with 14 cells as the tested pack in DST conditions to simulate the actual working process of a large battery pack. In Figure 6, the voltage prediction results of the CMM and cells are shown. Figure 6a shows the CMM voltage prediction results, and the corresponding errors are shown in Figure 6b. The prediction results of Bi-LSTM and ECM-RLS both show high accuracy with an error that is limited at around 2%, and the adaptive integrated prediction algorithm (abbreviated as AIP in the figure) results show the highest accuracy with an error that is below 0.450%. The cell voltage prediction results and errors are shown in Figure 6c,d. It can be seen that the voltage prediction error for every cell could be maintained below 1.5% in the DST conditions, which meets the application requirement.
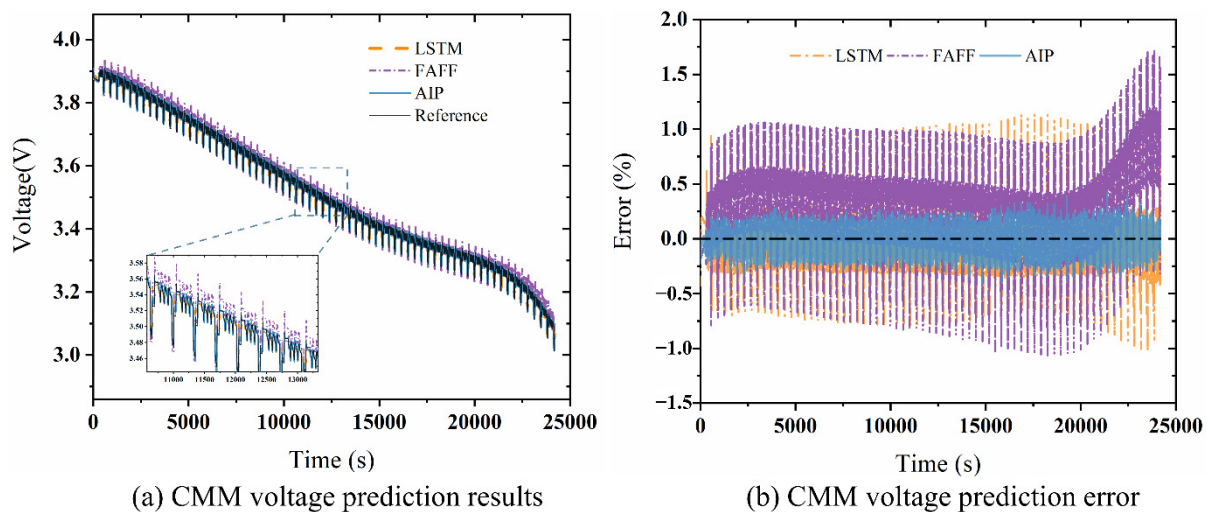

(a) CMM voltage prediction results　　　　(b) CMM voltage prediction error

Figure 6. *Cont.*

(c) Cell voltage prediction results
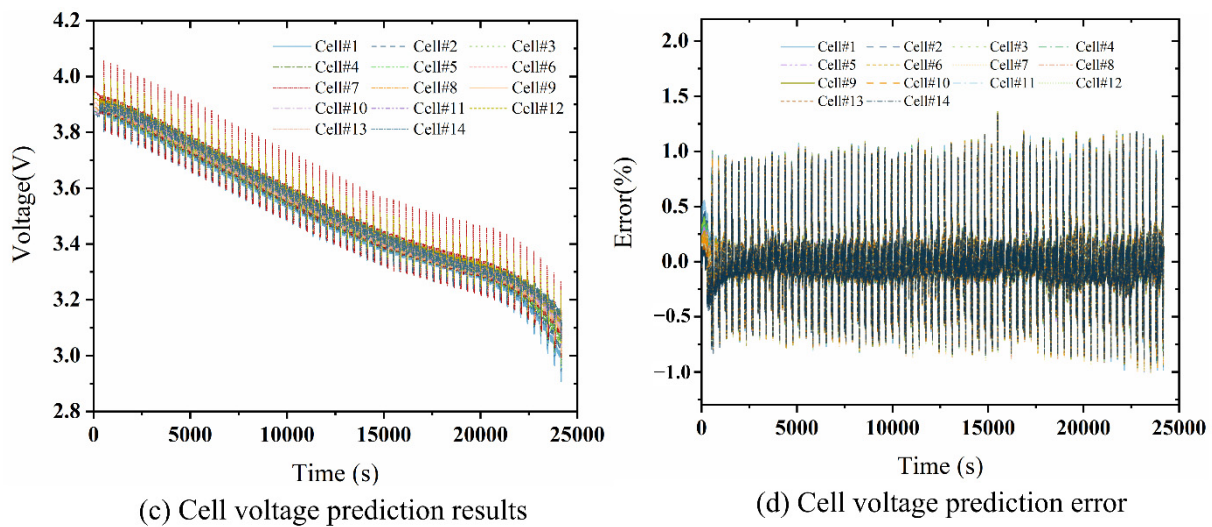
(d) Cell voltage prediction error

Figure 6. Voltage prediction on pack and cells in DST condition.

4. Results and Discussions

4.1. Data Sources

In this study, we use the actual vehicle data from the cloud platform to prove the accuracy of the proposed algorithm and the ISC detection performance of specific burning vehicles. The test data that were obtained from the actual vehicles were from ones that were driven in China, and the NMC battery pack of each vehicle contains 344 cells arranged in the configuration of 86S4P. Since four cells in parallel were equipped with one voltage sensor, every four cells in parallel were assumed to be a cell module in this paper. The data of five vehicles were mainly selected, including the data of three vehicles in normal operation and two vehicles that were reported as faulty vehicles, which was confirmed by a maintenance check. The data were collected by the sensor system of the vehicle BMS and uploaded at sampling intervals of 30s. The upload process of actual data was not continuous and only occurred when the vehicle BMS was online. We deployed a data cleaning process that was related to the quality of the online data, and its format during the signal deficiency was preprocessing. The time periods of the generation of the intercepted data was mainly conducted in 2021. In the following work, the start time of the intercepting data was recorded as "0" time, and the data were spliced at intervals of 30s.

4.2. Diagnosis Results on Real Vehicle Data

The adaptive integrated prediction algorithm combining Bi-LSTM and ECM-RLS is proposed in the above sections. In this section, we present the actual vehicle data from the cloud platform to prove the accuracy of the proposed algorithm and the ISC detection performance of specific burning vehicles. According to the previous work [10], there are many cases of ISCs, including ISCs that are due to extreme operating conditions such as a puncture and micro ISC due to lithium precipitation. For extreme cases of ISCs, the algorithm can achieve the advance monitoring of them in seconds and minutes. For the micro ISCs, the algorithm can achieve the advance detection of them in hours. In addition, the appearance of the ISC is different for different battery qualities and battery systems. As notes in this section, as for the NMC packs, the algorithm achieved prewarning more than 10 h in advance of the ISC occurring.

The proposed algorithm was tested by the data from three different normal vehicles in order to determine the practicability and accuracy of it under random working conditions. The chosen vehicles are three random taxis, which ensures the generalizability of the tested data. The intercepted data of the three vehicles were from different temperature domains, which can fully test the generality of the proposed method in different seasons and countries at different latitudes.

In this section, we use the actual vehicle data from the cloud platform to prove the accuracy of the proposed algorithm and the ISC detection performance of specific burning vehicles. The proposed algorithm was tested by the data from three different normal vehicles in order to check out the practicability and accuracy of it under random working conditions.

Figure 7a–c show the prediction results for the three normal vehicles at the temperature ranges of −5~10 °C, 10~20 °C, and 20~30 °C, respectively. In Figure 7, the data of no. 1 vehicle were intercepted at the temperature range of −5~10 °C from 5 January 2021 00:00:00 to 12 January 2021 18:00:00. The data of no. 2 vehicle were intercepted at the temperature range of 10~20 °C from 1 March 2021 00:00:00 to 7 March 2021 12:30:00. The data of no. 3 vehicle were intercepted at the temperature range of 20~30 °C from 15 April 2021 19:00:00 to 22 April 2021 09:00:00. In Figure 7a, compared with those of the no. 2 and the no. 3 vehicles, the battery consistency of the no. 1 vehicle is poorer. In addition, due to the temperature difference, the factors such as the driver's driving behavior, the load on electrical appliances, and the brake energy recovery have a subtle difference in their degree of influence on the voltage. The prediction results show that at different ambient temperatures and consistency levels, the voltage prediction error was limited at 3%. In Figure 7b,c, the prediction error on real voltage is also limited at 3%, and it was even lower when the battery pack attained high consistency, which attains the accuracy requirement.
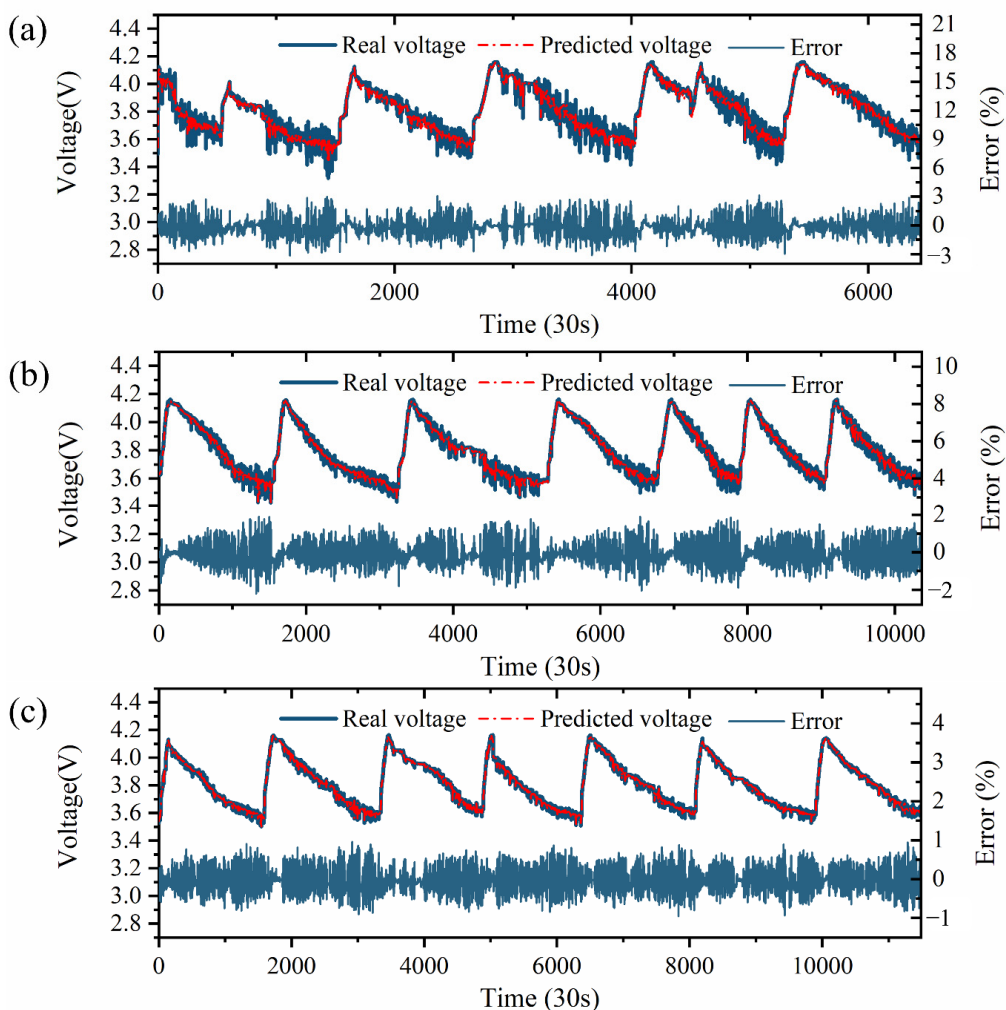

Figure 7. Voltage prediction results on different packs. (**a**) No.1 vehicle in the temperature range of −5~10 °C. (**b**) No.2 vehicle in the temperature range of 10~20 °C. (**c**) No.3 vehicle in the temperature range of 20~30 °C.

The no. 4 vehicle was identified as the defective sample, and the data were intercepted 10 h before the corrective maintenance was performed. The time range of the data in Figure 8 is from 15 February 2021 00:00:00 to 4 March 2021 16:44:40. The predicted and the real values of the voltage are shown in Figure 8. The dotted lines in Figure 8 of the predicted error are the thresholds of the three-stage alarm. Based on the analysis of the prediction error, the thresholds of the three fault levels were set, respectively. The primary alarm was used to distinguish between a normal car and a car with the potential for ISC. When this threshold is exceeded, the vehicle needs to be monitored in an engineering facility to analyze the cause. The vehicles that exceed this threshold may also be defined by other factors such as poor inconsistency. The follow-up monitoring of these vehicles is required. Triggering the secondary alarm means that the vehicle has a higher risk of an ISC occurring. This threshold will narrow the range of the vehicles with primary alarms, and such vehicles can be prioritized in an engineering monitoring facility due to the manpower and resource constraints. Triggering the tertiary alarm means there is a high probability that the battery has suffered an ISC, and these vehicles need to be recalled for service. Following the experts' experience, the primary alarm error is at 1.62% (the green dotted lines), the secondary alarm error is at 2.46% (the yellow dotted lines), and the tertiary alarm error is at 3.25% (the red dotted lines). As for the no. 4 vehicle, there is a trend of intermittent fault increase before it corrective maintenance was performed. In Figure 8, the cell prediction error triggered the tertiary alarm especially in the high discharge depth stage several times. In the discharge range at a low SOC, the prediction error of the no. 59 cell module is frequently at a very high level, which was far higher than that of other cells in the pack. These faulty cells (the no. 59 cell module) were proved to have incurred an ISC due to impurity that existed during the corrective maintenance.

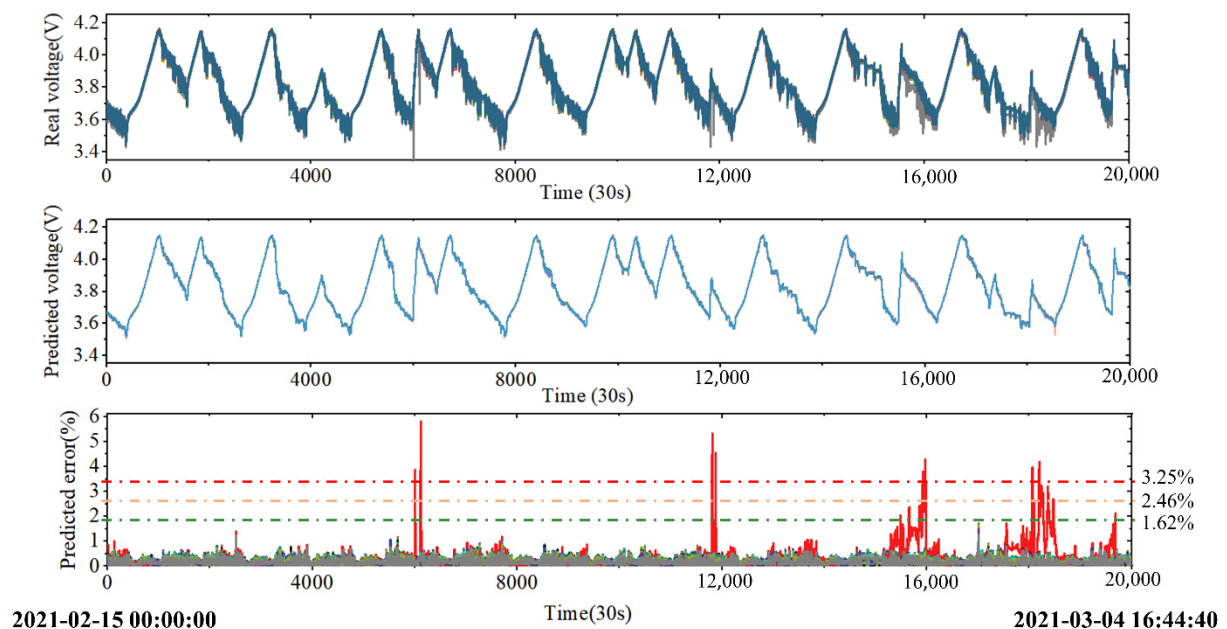Time range: 2021-02-15 00:00:00 to 2021-03-04 16:44:40

Figure 8. Battery voltage prediction results for no. 4 vehicle before corrective maintenance.

The no. 5 vehicle as chosen as the TR sample, and the data were intercepted 10 h before the steep increase in temperature and the pack valve ejection. The time range of the data in Figure 9 is from 1 April 2021 00:06:00 to 31 April 2021 16:18:00. In Figure 9, there was some sudden abnormal increase in the predicted error in the voltage prediction during the last three discharge cycles. The voltage prediction faulty severity triggered the primary and secondary alarms several times. Finally, at the 8500–9800 sampling time range (from 26 April 2021 14:20:00 to 31 April 2021 16:18:00), the tertiary alarm was triggered at two

periods. Compared with the no. 4 vehicle, the prediction error of the no. 5 one shows a gradually increasing trend, which reveals the deterioration process of the ISC in the battery. The diagnosis of the deterioration process can effectively realize the early warning of TR.

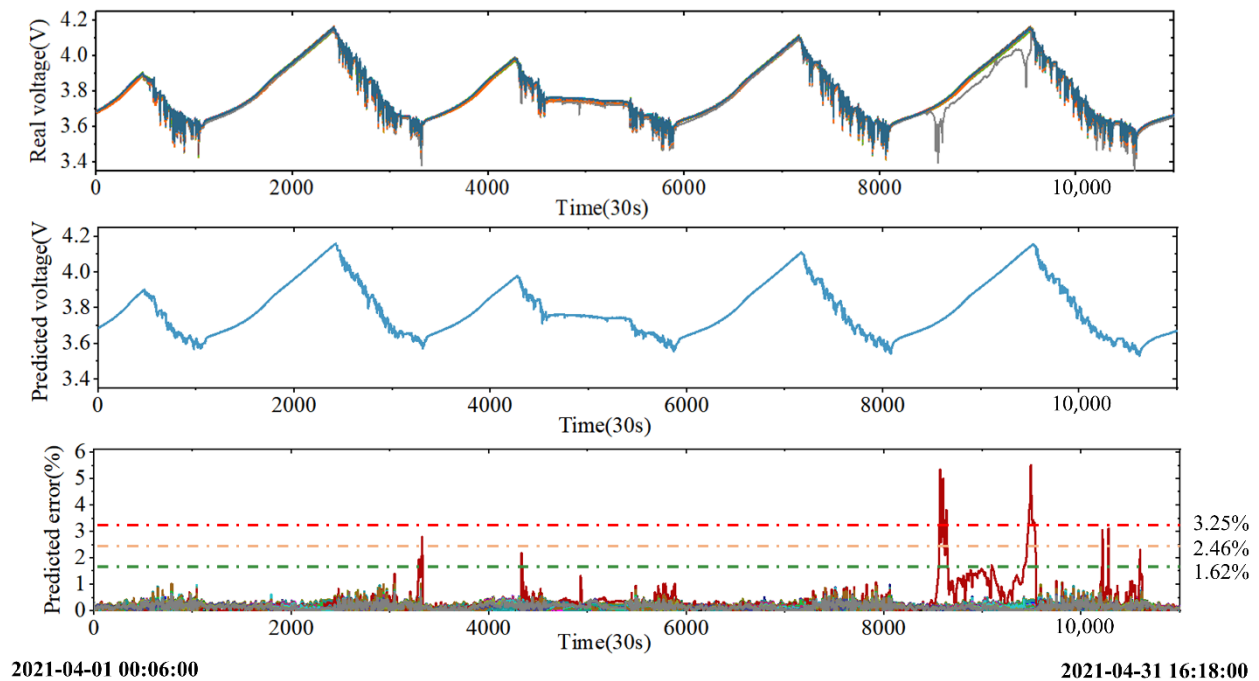Time range: 2021-04-01 00:06:00 to 2021-04-31 16:18:00

Figure 9. Battery voltage prediction results for no. 5 vehicle before TR.

5. Conclusions

In this work, the online ISC detection algorithm of the battery pack is proposed based on the online data from the cloud BMS. The modeling, state prediction, and ISC detection of the large battery packs in real vehicles were conducted. The MDM model was adopted for the modeling of large battery packs, in which the cell differences between the battery's internal impedance and SOC were taken into account in the deviation model. Compared with the traditional first-order equivalent circuit model, the identified parameters of the used model were reduced by 1/3, which at the same time significantly reduced the calculation difficulty and improved the robustness of the overall parameter identification. In the process of the MDM voltage prediction, the CMM voltage prediction network architecture was built based on the Bi-LSTM neural network. The input data of our proposed neural network contain the vehicle data collected by the cloud BMS, making up the lack of vehicle information in the previous battery equivalent circuit model. Finally, the AdaBoost algorithm was used to fuse the results of the neural network and the ECM-RLS prediction. The problems of instability of a single neural network and the low accuracy of ECM-RLS prediction are both solved. The final predicted voltage of each cell was obtained based on the corrected average state and the deviation state of the voltage prediction.

The final verification data of this work include the data of real vehicles and packs from the cloud BMS. The algorithm accuracy was verified by the data of three normal vehicles in different temperature ranges, and the three-level error threshold was determined according to the prediction error of the normal vehicles and expert experience. Finally, as it was tested by the data with a known ISC problem, the ISC judgment of the vehicles was realized. The algorithm was able to perform prewarning 10 h before the battery failure occurrence and TR in the test data. In actual working conditions, a battery failure is random and influenced by many factors. The ISC detection algorithm that is proposed in this paper can effectively identify the gradual ISC process in advance of it.

At present, battery management technology based on big data and cloud computing is booming. This research work can be used as a battery safety detection algorithm on the cloud-to-end collaboration framework, contributing to the online monitoring of electric vehicle battery safety. The battery ISC detection algorithm based on the voltage prediction that is proposed in this work will be continuously upgraded in the following application process. With an excellent decision-making ability, our algorithm will be more adaptive for different battery systems in future work.

Author Contributions: Conceptualization, R.C. and Z.Z.; methodology, R.C.; software, R.C. and X.L.; validation, J.L. (Jiayi Lu) and L.Z.; formal analysis, J.L. (Jiayi Lu); investigation, S.Y.; resources, S.Y.; data curation, X.L.; writing—original draft preparation, R.C.; writing—review and editing, X.L. and L.Z.; visualization, Z.Z.; supervision, J.L. (Jiayuan Lin) and L.X.; project administration, J.L. (Jiayuan Lin) and L.X.; funding acquisition, S.Y. All authors have read and agreed to the published version of the manuscript.

Conflicts of Interest: The authors declare no conflict of interest.

References

1. Hu, J.; Wei, Z.; He, H. An Online Adaptive Internal Short Circuit Detection Method of Lithium - Ion Battery. *Automot. Innov.* **2021**, *4*, 93–102. [CrossRef]
2. Wang, J.; Deng, Z.; Yu, T.; Yoshida, A.; Xu, L.; Guan, G.; Abudula, A. State of health estimation based on modified Gaussian process regression for lithium-ion batteries. *J. Energy Storage* **2022**, *51*, 104512. [CrossRef]
3. Liang, H.J.; Gu, Z.Y.; Zhao, X.X.; Guo, J.Z.; Yang, J.L.; Li, W.H.; Li, B.; Liu, Z.M.; Sun, Z.H.; Zhang, J.P.; et al. Advanced flame-retardant electrolyte for highly stabilized K-ion storage in graphite anode. *Sci. Bull.* **2022**, *67*, 1581–1588. [CrossRef]
4. Wan, H.; Zhang, J.; Xia, J.; Ji, X.; He, X.; Liu, S.; Wang, C. F and N Rich Solid Electrolyte for Stable All-Solid-State Battery. *Adv. Funct. Mater.* **2022**, *32*, 2110876. [CrossRef]
5. Zhu, X.; Chang, Z.; Yang, H.; He, P.; Zhou, H. Highly safe and stable lithium-metal batteries based on a quasi-solid-state electrolyte. *J. Mater. Chem. A* **2022**, *10*, 651–663. [CrossRef]
6. Liu, Y.; Gao, Y.; Zhi, J.; Huang, R.; Li, W.; Huang, X.; Yan, G.; Ji, Z.; Mai, W. All-inorganic lead-free NiOx/Cs3Bi2Br9 perovskite heterojunction photodetectors for ultraviolet multispectral imaging. *Nano Res.* **2022**, *15*, 1094–1101. [CrossRef]
7. Zhang, W.; Wang, L.; Wang, L.; Liao, C. Joint State-of-Charge and State-of-Available-Power Estimation Based on the Online Parameter Identification of Lithium-Ion Battery Model. *IEEE Trans. Ind. Electron.* **2022**, *69*, 3677–3688. [CrossRef]
8. Sun, Y.; Wang, Y.; Liu, Y.; Xiang, X. Highly Efficient Lithium Extraction from Brine with a High Sodium Content by Adsorption-Coupled Electrochemical Technology. *ACS Sustain. Chem. Eng.* **2021**, *9*, 11022–11031. [CrossRef]
9. Zhao, J.; Burke, A.F. Electric Vehicle Batteries: Status and Perspectives of Data-Driven Diagnosis and Prognosis. *Batteries* **2022**, *8*, 142. [CrossRef]
10. Feng, X.; Ouyang, M.; Liu, X.; Lu, L.; Xia, Y.; He, X. Thermal runaway mechanism of lithium ion battery for electric vehicles: A review. *Energy Storage Mater.* **2018**, *10*, 246–267. [CrossRef]
11. Maleki, H.; Howard, J.N. Internal short circuit in Li-ion cells. *J. Power Sources* **2009**, *191*, 568–574. [CrossRef]
12. Gao, W.; Zheng, Y.; Ouyang, M.; Li, J.; Lai, X.; Hu, X. Micro-short-circuit diagnosis for series-connected lithium-ion battery packs using mean-difference model. *IEEE Trans. Ind. Electron.* **2019**, *66*, 2132–2142. [CrossRef]
13. Huang, L.; Liu, L.; Lu, L.; Feng, X.; Han, X.; Li, W.; Zhang, M.; Li, D.; Liu, X.; Sauer, D.U.; et al. A review of the internal short circuit mechanism in lithium-ion batteries: Inducement, detection and prevention. *Int. J. Energy Res.* **2021**, *45*, 15797–15831. [CrossRef]
14. Gandoman, F.H.; El-shahat, A.; Alaas, Z.M.; Ali, Z.M.; Berecibar, M.; Aleem, S.H.E.A. Understanding Voltage Behavior of Lithium-Ion Batteries in Electric Vehicles Applications. *Batteries* **2022**, *8*, 130. [CrossRef]
15. Zhao, X.; Yang, H.; Wang, Y.; Sha, Z. Review on the electrochemical extraction of lithium from seawater/brine. *J. Electroanal. Chem.* **2019**, *850*, 113389. [CrossRef]
16. Hannan, M.A.; Lipu, M.S.H.; Hussain, A.; Mohamed, A. A review of lithium-ion battery state of charge estimation and management system in electric vehicle applications: Challenges and recommendations. *Renew. Sustain. Energy Rev.* **2017**, *78*, 834–854. [CrossRef]
17. Duan, B.; Li, Z.; Gu, P.; Zhou, Z.; Zhang, C. Evaluation of battery inconsistency based on information entropy. *J. Energy Storage* **2018**, *16*, 160–166. [CrossRef]
18. Shang, Y.; Lu, G.; Kang, Y.; Zhou, Z.; Duan, B.; Zhang, C. A multi-fault diagnosis method based on modified Sample Entropy for lithium-ion battery strings. *J. Power Sources* **2020**, *446*, 227275. [CrossRef]

19. Zheng, Y.; Han, X.; Lu, L.; Li, J.; Ouyang, M. Lithium ion battery pack power fade fault identification based on Shannon entropy in electric vehicles. *J. Power Sources* **2013**, *223*, 136–146. [CrossRef]
20. Wang, Y.; Tian, J.; Chen, Z.; Liu, X. Model based insulation fault diagnosis for lithium-ion battery pack in electric vehicles. *Meas. J. Int. Meas. Confed.* **2019**, *131*, 443–451. [CrossRef]
21. Schmid, M.; Gebauer, E.; Hanzl, C.; Endisch, C. Active Model-Based Fault Diagnosis in Reconfigurable Battery Systems. *IEEE Trans. Power Electron.* **2021**, *36*, 2584–2597. [CrossRef]
22. Li, D.; Zhang, Z.; Liu, P.; Wang, Z.; Zhang, L. Battery Fault Diagnosis for Electric Vehicles Based on Voltage Abnormality by Combining the Long Short-Term Memory Neural Network and the Equivalent Circuit Model. *IEEE Trans. Power Electron.* **2021**, *36*, 1303–1315. [CrossRef]
23. Zhao, Y.; Liu, P.; Wang, Z.; Zhang, L.; Hong, J. Fault and defect diagnosis of battery for electric vehicles based on big data analysis methods. *Appl. Energy* **2017**, *207*, 354–362. [CrossRef]
24. Yang, S.; He, R.; Zhang, Z.; Cao, Y.; Gao, X.; Liu, X. CHAIN: Cyber Hierarchy and Interactional Network Enabling Digital Solution for Battery Full-Lifespan Management. *Matter* **2020**, *3*, 27–41. [CrossRef]
25. Yang, S.; Zhang, Z.; Cao, R.; Wang, M.; Cheng, H.; Zhang, L.; Jiang, Y.; Li, Y.; Chen, B.; Ling, H.; et al. Implementation for a cloud battery management system based on the CHAIN framework. *Energy AI* **2021**, *5*, 100088. [CrossRef]
26. Zheng, Y.; Ouyang, M.; Lu, L.; Li, J.; Han, X.; Xu, L.; Ma, H.; Dollmeyer, T.A.; Freyermuth, V. Cell state-of-charge inconsistency estimation for LiFePO4 battery pack in hybrid electric vehicles using mean-difference model. *Appl. Energy* **2013**, *111*, 571–580. [CrossRef]
27. Feng, F.; Hu, X.; Liu, K.; Che, Y.; Lin, X.; Jin, G.; Liu, B. A Practical and Comprehensive Evaluation Method for Series-Connected Battery Pack Models. *IEEE Trans. Transp. Electrif.* **2020**, *6*, 391–416. [CrossRef]
28. Fan, S. Fault Diagnosis Method based on Method based based on Stacked Stacked. *IFAC Pap.* **2020**, *53*, 790–795. [CrossRef]
29. Liu, K.; Shang, Y.; Ouyang, Q. A Data-Driven Approach With Uncertainty Quantification for Predicting Future Capacities and Remaining Useful Life of Lithium-ion Battery. *IEEE Trans. Ind. Electron.* **2021**, *68*, 3170–3180. [CrossRef]
30. Carkhuff, B.G.; Demirev, P.A.; Srinivasan, R. Impedance-Based Battery Management System for Safety Monitoring of Lithium-Ion Batteries. *IEEE Trans. Ind. Electron.* **2018**, *65*, 6497–6504. [CrossRef]
31. Chemali, E.; Member, S.; Kollmeyer, P.J.; Preindl, M.; Ahmed, R.; Emadi, A. Long Short-Term Memory Networks for Accurate State-of-Charge Estimation of Li-ion Batteries. *IEEE Trans. Ind. Electron.* **2018**, *65*, 6730–6739. [CrossRef]
32. Wang, G.; Gao, Q.; Yan, Y.; Wang, Y. Thermal Management Optimization of a Lithium - Ion Battery Module with Graphite Sheet Fins and Liquid Cold Plates. *Automot. Innov.* **2020**, *3*, 336–346. [CrossRef]
33. Wang, W.; Sun, D. The improved AdaBoost algorithms for imbalanced data classification. *Inf. Sci.* **2021**, *563*, 358–374. [CrossRef]